Accepted Manuscript

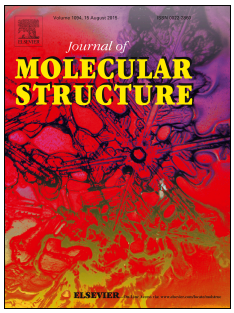

Synthesis, crystal structure, spectral and DFT studies of potent isatin derived metal complexes

Sajjad Hussain Sumrra, Aftab Hussain Atif, Muhammad Naveed Zafar, Muhammad Khalid, Muhammad Nawaz Tahir, Muhammad Faizan Nazar, Muhammad Arif Nadeem, Ataualpa A.C. Braga

PII: S0022-2860(18)30429-0

DOI: 10.1016/j.molstruc.2018.03.132

Reference: MOLSTR 25071

To appear in: *Journal of Molecular Structure*

Received Date: 18 August 2017

Revised Date: 28 March 2018

Accepted Date: 30 March 2018

Please cite this article as: S.H. Sumrra, A.H. Atif, M.N. Zafar, M. Khalid, M.N. Tahir, M.F. Nazar, M.A. Nadeem, A.A.C. Braga, Synthesis, crystal structure, spectral and DFT studies of potent isatin derived metal complexes, *Journal of Molecular Structure* (2018), doi: 10.1016/j.molstruc.2018.03.132.

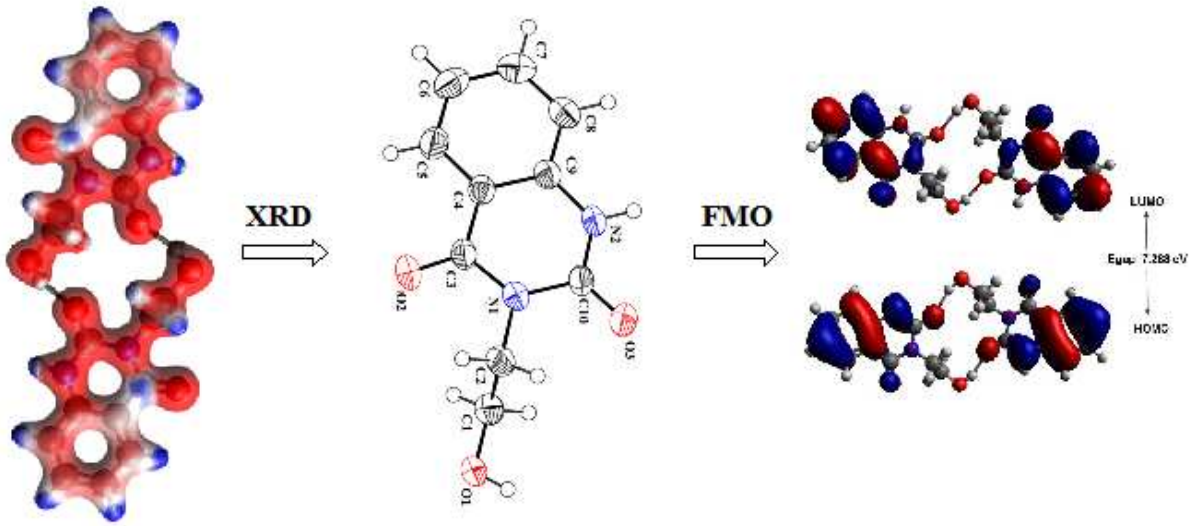

Synthesis, Crystal Structure, Spectral and DFT Studies of Potent Isatin Derived Metal Complexes

Sajjad Hussain Sumrra*[1], Aftab Hussain Atif[1], Muhammad Naveed Zafar[2], Muhammad Khalid*[3], Muhammad Nawaz Tahir[4], Muhammad Faizan Nazar[1], Muhammad Arif Nadeem[5], Ataualpa A. C. Braga[6]

[1]*Department of Chemistry, University of Gujrat 50700, Pakistan.*
[2]*Department of Chemistry, Quaid-i-Azam University, Islamabad 45320, Pakistan.*
[3]*Department of Chemistry, Khwaja Fareed University of Engineering & Information Technology, Rahim Yar Khan, Pakistan.*
[3]*Department of Chemistry, University of Education Lahore, Faisalabad Campus, Pakistan.*
[4]*Department of Physics, University of Sargodha, Sargodha, Pakistan.*
[5]*Department of Chemistry, University of Gujrat 50700, Pakistan.*
[6]*Departamento de Química Fundamental, Instituto de Química, Universidade de São Paulo, Av. Prof. LineuPrestes, 748, São Paulo, 05508-000, Brazil*

ABSTRACT

The isatin-core in compounds offers exciting perspectives in medicinal and pharmacological research. The present study reports the successful development of new isatin-core transition metal based anti-bacterial complexes *via* conventional refluxing method. The bidentate nature of as-synthesized isatin-core ligand was confirmed using various analytical techniques such as FTIR, ^{1}H NMR, ^{13}C NMR, EIMS, and single crystal X-ray diffraction. The computed analysis i.e. IR, UV-Visible, NBO (Natural Bond Orbital) and FMO (Frontier Molecular Orbital) of crystalline isatin-core ligand reflect its dimer nature and predict the conjugative interaction among molecules. Moreover, metal complexes of isatin-core ligand using metallic salts of first transition series i.e. VO(IV), Cr(III), Mn(II), Fe(II), Co(II), Ni(II), Cu(II) and Zn(II) were prepared and further screened against bacterial strains. Octahedral geometry was proposed for all the complexes except vanadium which had square-pyramidal geometry. All the as-prepared metal complexes are found potentially active entities against both of the gram-positive and gram-negative bacterial strains. Additionally, the bacterial screened data revealed that metal complexes have better bactericidal activities compared to their parent ligand.

Keywords: Bidentate Ligand, Metal Chelates, Computed Analysis, Conjugative Interaction, Bactericidal

* Corresponding authors E-mail address: sajjadchemist@uog.edu.pk (Sajjad Hussain Sumrra)
muhammad.khalid@kfueit.edu.pk (Muhammad Khalid)

Introduction

Isatin (1*H*-Indole-2,3-dione) is a natural compound found in most plants. It is a unique class of heterocycles acting as biological agents [1]. Isatin derived compounds have extensive applications in the pharmacological and medicinal field due to the presence of bioactive indole moiety containing both keto and lactum groups [2-5]. Isatin and its derivatives have a number of biological applications including nervous system activities and as a metabolic derivatives of humans [6, 7]. Isatin and its derived compounds also possess broad range of pharmacological effects [8], such as antifungal [9, 10], antibacterial [11, 12], anti HIV [13] and antiviral [14-16]. Isatin also shows enzyme inhibition activity [17, 18] and act as cytotoxic agent against tumor cells [19-22]. Moreover, Isatin derived compounds have a number of actions in the brain against different types of infections [23]. It also exhibit antiproliferative [24] and caspase inhibitor activities [25, 26]. Compounds of isatin possess SARS protease [27], antismall pox [28], kinase activator [29], and inflammatory activities [30]. These biological functions validated isatin as a starting point for the design and preparation of chemical libraries [31, 32]. Metal complexes of isatin based ligands attracted much attention nowadays because of their diagnostic and therapeutic properties [33]. Copper (II) complexes of isatin based ligand are used as antimicrobial agents [34]. Cobalt complexes derived from isatin ligands possess good antibacterial activity against different strains of bacteria [24]. These versatile functions of isatin based compounds and their complexes compelled us to extend this chemistry and synthesize new compound, 3-(2-hydroxyethyl)quinazoline-2,4(1*H*,3*H*)-dione (**E9**) by reacting isatin with ethanolamine and its metal complexes with transition metals (V, Cr, Mn, Fe, Co, Ni, Cu and Zn). The DFT calculations are being performed for ligand to check the molecular interactions in a compound and its stability. Finally, antibacterial activity against different bacterial strains has been performed for all the synthesized compounds.

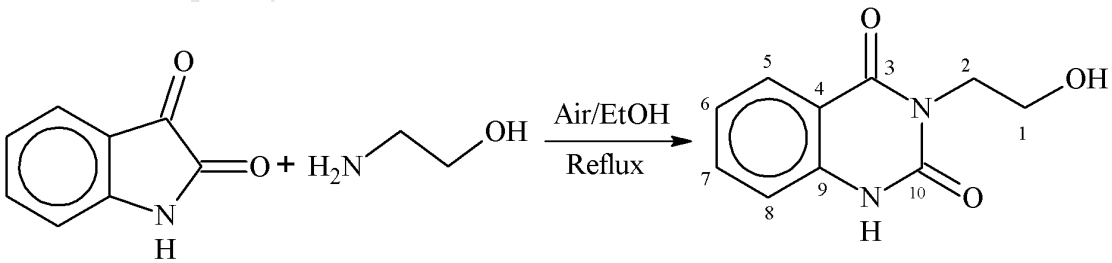

Scheme 1: Synthesis of 3-(2-hydroxyethyl)quinazoline-2,4(1*H*,3*H*)-dione (E9)

Results and Discussion

The reaction of 1*H*-Indole-2,3-dione with ethanolamine in an equimolar ratio afforded brown color product **(Scheme 1)**. The brown crystals of isatin based ligand were grown successfully. The compound was moisture and air stable, soluble in methanol and DMSO. The melting point of the compound was 248ºC. The bidentate isatin based ligand reacted readily with first series of following transition metals; VO(IV), Cr(III), Mn(II), Fe(II), Co(II), Ni(II), Cu(II) and Zn(II) to form metal complexes (**Scheme 2-4**).

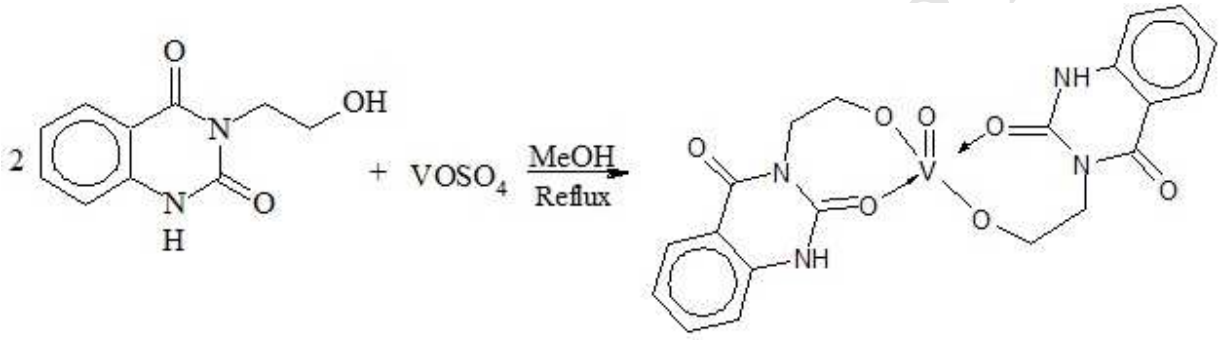

Scheme 2: Synthesis of Oxovanadium(IV) Complex

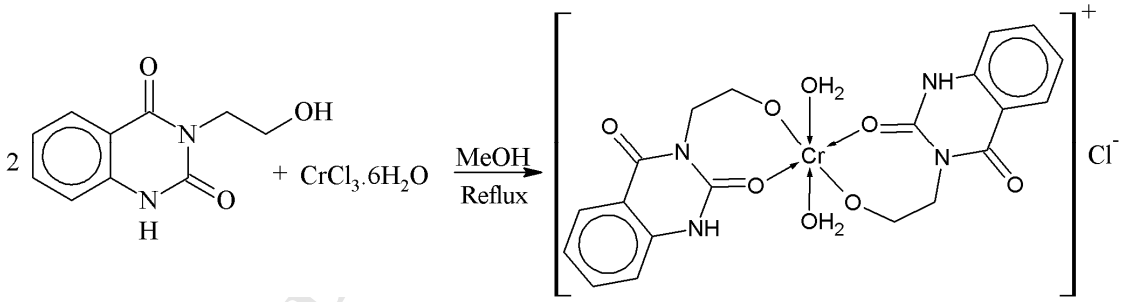

Scheme 3: Synthesis of Chromium(III) Complex

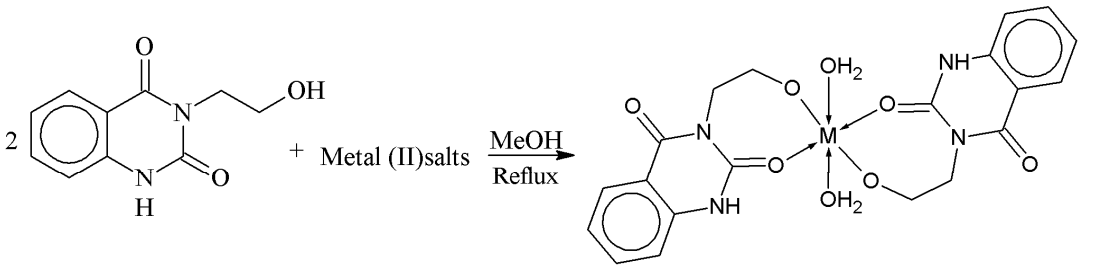

M= Mn(II), Fe(II), Co(II), Ni(II), Cu(II) and Zn(II)

Scheme 4: Synthesis of Metal(II) Complexes

All the metal complexes were intensely colored except Zn(II) and Cr(III) which were of off white color. All the complexes were soluble in DMSO and having decomposition temperature in the range 258-290 except Fe(II) which showed greater than 300ºC.

^{1}H NMR of E9

The proton NMR spectrum was recorded using DMSO-d_6 as a solvent. The careful study of spectrum (**Table 1**) demonstrated one signal of proton as singlet at 11.32 ppm confirming the presence of N-H proton. Two signals appeared as triplet at 3.54-3.99 ppm for four CH_2 aliphatic protons indicating the presence of ethyl group of ethanolamine. The isatin aromatic protons were appeared as multiplet at 7.15-7.93 ppm. The O-H proton appeared at 4.72 ppm. These all proton signals supported the proposed structure of E9 [35].

Table 1. ^{1}H NMR Data of E9

Sr. #	Position of peak	Signal values (ppm)
1	N-H proton	11.32 (s, 1H)
2	Aliphatic protons	3.54-3.99 (t, 4H)
3	Aromatic protons	7.15-7.93 (m, 4H)
4	O-H proton	4.72 (s, 1H)

s = singlet, t = triplet, m = multiplet

^{13}C NMR of E9

The ^{13}C NMR spectrum of ligand was recorded in DMSO solvent. The examination of spectrum revealed that the signal of C_2 appeared at 42 ppm and a downfield signal at 57.6 ppm appeared due to attachment of OH group at C_1. The six signals displayed between 113-139 ppm were due to the presence of phenyl carbons (C_4-C_9) of isatin moiety. Due to the electronegative effect of oxygen and inductive effect of nitrogen, C_3 carbon appeared as downfield at 150.2 ppm. The

downfield shift of C_{10} at 162 ppm was observed indicating the presence of C=O carbon. This downfield shift was also due to attachment of electronegative oxygen and nitrogen atoms. All the carbon peaks were in good agreement with proposed structure [35].

Mass Spectrum of E9

The mass fragmentation pattern of E9 compound is showed the existence of molecular ion peak at m/z = 206 which indicated the formation of said compound. The base peak of 100% intensity was observed at m/z = 163, by the loss of all three oxygen from parent compound through C-O and C=O bond cleavage. The other mass fragments formed as shown in figure were produced by the cleavage of C-C, C-O, C=O, C-N bonds.

Single Crystal Analysis of E9

The data in **Table 2** showed that all the bond lengths and angles were within normal range. Hydrogen bonding in **Table 2** and **Figure 2** showed that two types of intermolecular hydrogen bonding O1—H1···O3 and N2—H2···O1 were present in crystal structure forming dimer and stabilizing the crystal molecular system.

The solid state structure of E9 was resolved using X-ray diffraction technique (**Table 2**). ORTEP diagram of single molecule and unit cell packing are given in **Figure 1** and **2,** respectively. The selected bond lengths, bond angles, torsion angles and H-bonding are shown in **Table 3**.

Table 2. Crystal Data of E9 Compound

Crystal data	**Compound (E9)**
CCDC	1515138
Chemical formula	$C_{10}H_{10}N_2O_3$
M_r	206.20
Crystal system, space group	Monoclinic, $P2_1/c$
Temperature (K)	296
a, *b*, *c* (Å)	13.1382 (16), 4.7630 (5), 14.9136 (19)
β (°)	95.035 (4)
V (Å^3)	929.65 (19)
Z	4
Radiation type	Mo $K\alpha$
μ (mm^{-1})	0.11
Crystal size (mm)	0.45 × 0.22 × 0.18
Data collection	
Diffractometer	Bruker Kappa APEXII CCD
Absorption correction	Multi-scan (*SADABS*; Bruker, 2005)
No. of measured, independent and observed [$I > 2\sigma(I)$] reflections	7771, 2012, 1546
R_{int}	0.026
$(\sin \theta/\lambda)_{max}$ (Å^{-1})	0.639
Refinement	
$R[F^2 > 2\sigma(F^2)]$, $wR(F^2)$, S	0.060, 0.177, 1.21
No. of reflections	2012
No. of parameters	138
H-atom treatment	H-atom parameters constrained
$\Delta\rangle_{max}$, $\Delta\rangle_{min}$ (e Å^{-3})	0.90, -1.02

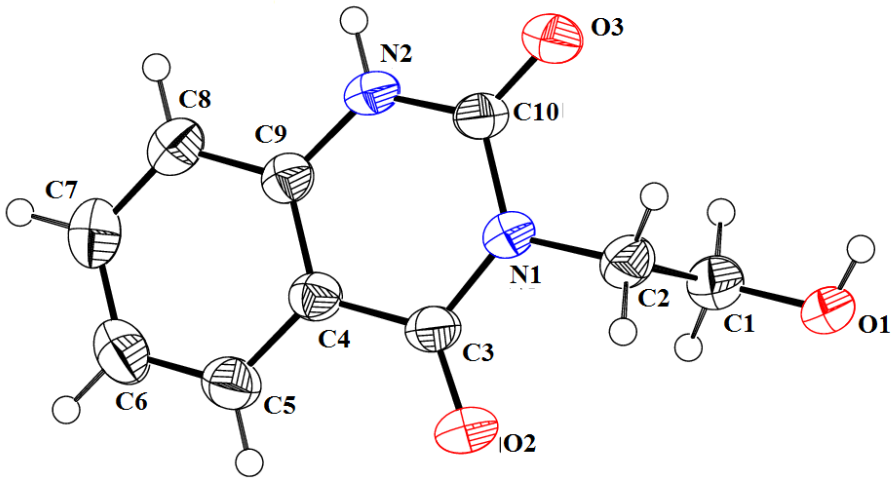

Figure 1. ORTEP Diagram of Single Unit of E9

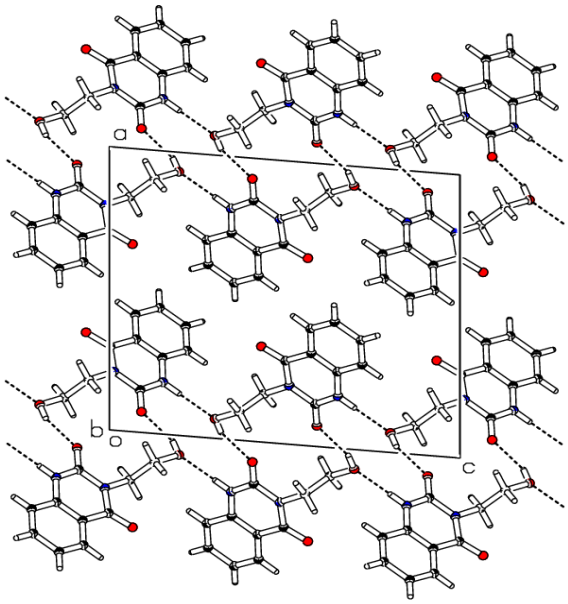

Figure 2. Unit Cell Packing of E9

Table 3. Hydrogen Bond Parameters (Å) of Ligand (E9)

D—H···*A*	*D*—H (Å)	H···*A* (Å)	*D*···*A* (Å)	*D*—H···*A* (°)
O1—H1···O3^{i}	0.82	1.98	2.7242 (17)	151.1
N2—H2···O1^{ii}	0.86	1.95	2.7953 (17)	168.6

Symmetry code(s): (i) −*x*, −*y*+2, −*z*; (ii) *x*, −*y*+3/2, *z*+1/2.

DFT Calculations of E9 Crystal

Computed and Experimental FT-IR Characterization of E9

The experimental and theoretical frequencies along with intensity and vibrational assignment are given in **Table 4**.Vibrational frequencies of E9 compound were designed with the help of DFT/B3LYP with 6-31G(d,p) basis set.

C-H Vibrations

The C-H stretching vibrations of the aromatic ring are commonly observed in the 3000-3100 cm^{-1} region of FT-IR spectrum [36], and are easily predicted using DFT frequencies. The experimental C-H stretching frequencies of E9 ligand are observed at 3150 and 3100 cm^{-1}, which are in good agreement with scaled frequencies at 3105 and 3081 cm^{-1}. The small differences between DFT and experimental frequencies are maybe due to interactions in the solid state sample used for spectral data, and no interactions in gaseous sample used for DFT calculations. The C-H bending vibrations are usually observed in 1000-1300 cm^{-1} region [37]. The weak to medium bending bands are observed at 1100, 1150 and 1200 cm^{-1} in spectral data, these bands are well correlated to the computed bands predicted at 1096, 1146 and 1192 cm^{-1}. These bands are actually C-H bending rocking vibrations coupled with scissoring vibrations. The C-H aliphatic bands are observed at 2930 and 2980 cm^{-1} resulted from the symmetric stretch of aliphatic CH_2 group in the compound, these vibrations are supported by computed frequencies

appeared at 2926 and 2992 cm^{-1} showing good correlation between spectral and theoretical results. The banding vibrations of CH_2 appeared at 1330 and 1350 cm^{-1} as medium bands in the experimental data, these frequencies are due to rocking and twisting bending modes. The computed frequencies at 1323 and 1350 cm^{-1} supported the spectral bending modes (**Table 4**).

Ring Vibrations

Stretching vibrations of C-C in a ring generally appeared at 1430-1650 cm^{-1}. FT-IR vibrations appeared at 1550 and 1600 cm^{-1} as weak bands are in good agreement with computed data at 1580 and 1600 cm^{-1} showing of carbon-carbon single and double bond vibrations (**Table 4**).

N-H Vibrations

N-H stretching vibration at 3200 cm^{-1} as weak band is appeared in the spectral data, the computed vibration was at 3506 cm^{-1}. The N-H bending vibration is observed at 1400 cm^{-1} as weak band in experimental showing rocking vibrations, well agreed with computational band at 1402 cm^{-1} (**Table 4**).

C=O Vibrations

The C=O stretching vibration are appeared at 1650, 1700 cm^{-1} as strong band in the spectral data, and these bands are fully supported by DFT vibrations at 1663, 1708 cm^{-1}. It is interesting to note that these vibration are mixed with other mode of vibrations appeared in the same region (**Table 4**).

Hydrogen Bond Vibrations

It is well known that spectral frequency of O-H is always decreased from expected value during intermolecular hydrogen bonding [38]. The O-H symmetric stretching vibration is observed at 3430 cm^{-1} as medium broad band, not correlated with computed band appeared at 3706 cm^{-1},

downward shift in frequency indicating the presence of intermolecular hydrogen bonding in dimer form. The O-H bending vibration is observed experimentally at 1050 cm^{-1} as strong band, and theoretically at 1088 cm^{-1} due to the rocking bending mode of vibration. The difference between actual and theoretical frequency may be assigned to intermolecular hydrogen bonding. The **Figure 3** clearly shows the presence of O-H···O hydrogen bonding in dimer, as in dimer form the intensity of band of O-H in monomer at 3706 cm^{-1} increased and frequency is shifted downward. This increase in intensity along with decrease in frequency of the dimer form as compared to the monomer form, what clearly indicate the presence of O-H···O hydrogen bonds.

Table 4. Experimental and Theoretical Frequencies of IR along with Intensity and Vibrational Assignment

Frequency Scaled	Experimental	I_{IR}	Vibrational assignments
1088	1050s	13.426	δ C-$H_{Aromatic}$ + ρO-H + αC-$H_{aliphatic}$
1096	1100m	12.3653	δ C-$H_{Aromatic}$ + ρO-H + αC-$H_{aliphatic}$
1139	1145	6.9042	δ C-$H_{Aromatic}$ + υC-N
1146	1150m	14.7788	δ C-$H_{Aromatic}$
1192	1200w	10.3409	δ C-$H_{Aromatic}$ + ρN-H
1229		17.981	δ C-$H_{Aromatic}$ + ρN-H + αC-$H_{aliphatic}$
1242	1250m	37.2941	δ C-$H_{Aromatic}$ + ρN-H + αC-$H_{aliphatic}$
1253		10.2608	ρC-$H_{Aromatic}$
1306	1300w	15.6821	ρC-$H_{Aliphatic}$
1314		8.4198	ρC-$H_{Aromatic}$ + ρC-$H_{Aliphatic}$
1323	1330m	12.2977	ρC-$H_{Aliphatic}$
1350	1350m	172.9735	αC-$H_{aliphatic}$ + ρO-H
1365		60.6736	ρC-$H_{Aromatic}$ + ρC-$H_{Aliphatic}$ + ρO-H
1385		123.1791	ρC-$H_{Aromatic}$ + ρC-$H_{Aliphatic}$
1402	1400m	31.4672	ρC-$H_{Aromatic}$ + ρN-H
1423		59.9851	δ C-$H_{Aliphatic}$
1463	1450s	3.772	δ C-$H_{Aliphatic}$
1478		81.2011	ρC-$H_{Aromatic}$
1481	1500w	55.5871	ρC-$H_{Aromatic}$
1580	1550w	17.2222	υ(s)C-C=C + δC-C=C

1600	1600w	119.8445	δ C-H$_{\text{Aromatic}}$ + ρN-H
1663	1650s	687.0003	υ(s)C=O + ρN-H + δ C-H$_{\text{Aliphatic}}$
1708	1700s	457.6824	υ(s)C=O + ρN-H + δ C-H$_{\text{Aliphatic}}$
2926	2930m	30.4821	υ(s)C-H$_{\text{Aliphatic}}$
2992	2980m	12.3452	υ(s)C-H$_{\text{Aliphatic}}$
3004		15.9051	υ(as)C-H$_{\text{Aliphatic}}$
3052		1.1975	υ(as)C-H$_{\text{Aliphatic}}$
3067	3100w	3.4707	υ(as)C-H$_{\text{Aromatic}}$
3081	3150w	7.7816	υ(as)C-H$_{\text{Aromatic}}$
3092		5.3436	υ(as)C-H$_{\text{Aromatic}}$
3105		5.3392	υ(s)C-H$_{\text{Aromatic}}$
3508	3400w	68.6926	υ(s)N-H
3706	3430m	37.4498	υ(s)O-H

Frequencies are given in cm^{-1}, υ = stretching, α=twisting, δ =scissoring, ρ =rocking, s=symmetric, as=asymmetric, w= weak, m= medium, s= strong.

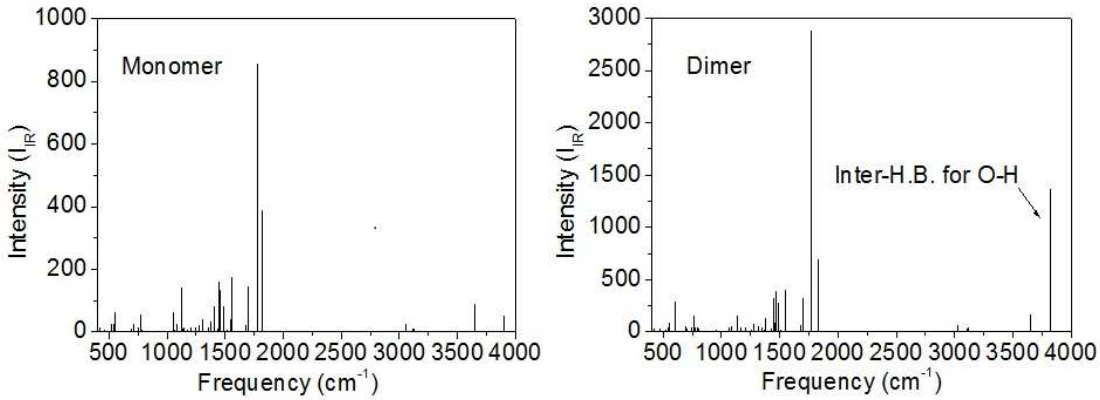

Figure 3. FT-IR Absorption Spectra Calculated at B3LYP/6-31G(d,p) Level of Theory

NBO Analysis of E9

It is well known that NBO analysis is a handy tool for measuring molecular interaction among molecules. These are mostly hyper conjugative interactions, charger transfer and hydrogen bonding. In these interactions the electron density transfer from donor orbital to acceptor orbital and give stabilization energy to whole of the system. The magnitude of interactions is related to values of stabilization energy, greater values of energy show more interactions among molecular

system [39]. **Table 5** shows the NBO donor and acceptor orbital along with stabilization energy values. The charge transfer from σ (O29-C50)→ σ^*(C45-H46) and σ (O29-C50)→ σ^*(C47-H48) shows the larger stabilization energy values of 99.49 and 89.59 kJ/mol respectively, indicating strong conjugative interaction between C-O bonding to C-H antibonding sigma orbital. In the similar way the electron transfer from σ (N31-C50)→ σ^*(C45-H46) and σ (N30-C50)→ σ^*(C47-H48) give stabilization energy of 66.78 and 53.26 kJ/mol respectively. The charge transfer from π bonding orbital to π^* antibonding orbital gives stabilization energy values of 32.96 and 31.98 kJ/mol for C16-C18→ C20-C22 and C20-C22→ C15-C24, respectively, these interactions are due to the π electron delocalization in a system. The interaction between lone pair 1 (O4), lone pair 2 (O4), lone pair 1 (O29) and lone pair 2 (O29) to antibonding σ^* O26-H27, O26-H27, O1-H2 and O1-H2 give stabilization energies of 5.01, 2.35, 5.04 and 2.38 kJ/mol, respectively, indicating the presence of intermolecular O-H···O hydrogen bonding. The interaction of lone pair 2 (O3) and lone pair 2 (O4) to σ^* (N5-C14) and (N5-C25) give stabilization values of 34.68 and 28.93 kJ/mol respectively showing conjugative interaction between O to C-N. The interaction of lone pair 1 (N5), lone pair 1 (N6) and lone pair 1 (N30) to π^* (O4-C25), (O4-C25) and (O29-C50) give stabilization energies of 69.97, 66.32 and 70.04 kJ/mol respectively showing hyper conjugative interaction in which charge delocalization occur from lone pair of N to C-O bond. The charge transfer between lone pair 2 (O28) and lone pair 1 (O29) to antibonding σ^* (C39-C40) and (C47-H48) give stabilization energy values of 21.32 and 50.68 kJ/mol, respectively, indicating conjugative interaction between O to C-C and O to C-H. The NBO analysis shows that molecular system contain O-H···O hydrogen bonding and strong conjugative interactions (**Table 5**).

Table 5. NBO analysis of E9 with Second-Order Perturbation Theory

Donor NBO (i)	Type	Acceptor NBO (j)	Type	$E^{(2)a}$ (kj/mol)	E(j) - E(i)[b] (a.u.)	F(i,j)[c] (a.u.)
C15-C24	π	O3-C14	π^*	25.44	0.38	0.089
C15-C24	π	C16-C18	π^*	28.28	0.38	0.094
C16-C18	π	C20-C22	π^*	32.96	0.35	0.097
C20-C22	π	C15-C24	π^*	31.98	0.35	0.098
O3	LP (2)	N5-C14	σ^*	34.68	0.79	0.149
O4	LP (2)	N5-C25	σ^*	28.93	0.82	0.139
N5	LP (1)	O3-C14	π^*	59.25	0.37	0.137
N5	LP (1)	O4-C25	π^*	69.97	0.37	0.143
N6	LP (1)	O4-C25	π^*	66.32	0.39	0.145
N6	LP (1)	C15-C24	π^*	46.4	0.38	0.122
O4	LP (1)	O26-H27	σ^*	5.01	1.37	0.074
O4	LP (2)	O26-H27	σ^*	2.35	0.91	0.043
O29	LP (1)	O1-H2	σ^*	5.04	1.37	0.074
O29	LP (2)	O1-H2	σ^*	2.38	0.91	0.043
O29-C50	σ	C45-H46	σ^*	99.49	4.29	0.584
O29-C50	σ	C47-H48	σ^*	89.59	4.21	0.549
N30-C36	σ	C47-H48	σ^*	27.07	3.88	0.29
N30-C39	σ	C45-H46	σ^*	20.85	4.05	0.26
N30-C50	σ	C47-H48	σ^*	53.26	3.99	0.412
N31-H32	σ	C45-H46	σ^*	27.03	3.92	0.291
N31-C49	σ	C47-H48	σ^*	20.37	4	0.255
N31-C50	σ	C45-H46	σ^*	66.78	4.08	0.466
C40-C49	π	C41-C43	π^*	28.28	0.38	0.094
C41-C43	π	C45-C47	π^*	31.78	0.37	0.097
O28	LP (2)	N30-C39	σ^*	34.4	0.79	0.149
O28	LP (2)	C39-C40	σ^*	21.32	0.86	0.123
O29	LP (1)	C45-H46	σ^*	46.19	3.96	0.383
O29	LP (1)	C47-H48	σ^*	50.68	3.88	0.397
O29	LP (2)	N30-C50	σ^*	30.63	0.82	0.144
O29	LP (2)	N31-C50	σ^*	30.25	0.84	0.144
O29	LP (2)	C45-H46	σ^*	33.2	3.51	0.314
O29	LP (2)	C47-H48	σ^*	26.89	3.42	0.279
N30	LP (1)	O28-C39	π^*	59.24	0.37	0.137
N30	LP (1)	O29-C50	π^*	70.04	0.37	0.143
N31	LP (1)	O29-C50	π^*	66.13	0.39	0.145
N31	LP (1)	C40-C49	π^*	46.35	0.39	0.123

a $E^{(2)}$ means energy of hyper conjugative interaction (stabilization energy).

b Energy difference between donor and acceptor i and j NBO orbital.

c F(i, j) is the Fork matrix element between i and j NBO orbital.

UV Visible Analysis of E9

In the experimental graph the maximum obtained at 264 nm indicated the presence of HOMO→ LUMO (90%) transition as calculated by computational analysis and this is due to π to π^* transition in a compound. There are some other transitions which were calculated using computational analysis are shown in **Table 6**.

Table 6. Experimental and Calculated Electronic Bands for E9

Experimental wavelength (nm)	Calculated wavelength (nm)	Oscillator strength (f)	Major contribution (%)
264	264	0.068	H-2→ L+2 (3%), H-1→ L+2 (5%), H→ L (90%)
	250	0.001	H-5→ L (7%), H-3→ L (68%), H-3→ L+9 (10%), H-3→ L+13 (3%)
	224	0.015	H-2→ L (7%), H-1→ L (28%), H→ L+2 (58%)
	214	0.0001	H→ L+1 (86%), H→ L+3 (4%), H→ L+5 (3%)
	202	0.204	H-4→ L (3%), H-2→ L (78%), H→ L+2 (8%), H→ L+9 (3%)
	201	0.796	H-1→ L (62%), H→ L+2 (28%)

Frontier Molecular Orbital of E9

The frontier molecular orbital theory is very helpful to calculate electric and optical parameters. In this, HOMO orbital acts as donor and LUMO as electron acceptor. The excitation of electron occurs from HOMO to LUMO. **Figure 4-6** shows frontier HOMO and LUMO orbitals surfaces with energy gap between occupied and unoccupied orbital. The energies for HOMO and LUMO are calculated as -8.283 eV and -0.996 eV, respectively. The orbital energies of HOMO-1 and LUMO+1 are -8.284 *eV* and -0.992 eV, respectively. The energies -8.854 eV and -0.181 eV belongs to HOMO-2 and LUMO+2 orbitals. In HOMO and HOMO-1 orbital, the electron density is mainly delocalized on phenyl ring and N-H of E9 compound, where, as in HOMO-2, the electrons are delocalized through the nitrogen, oxygen and methylene groups. In LUMO and LUMO+1 orbital, electrons are delocalized on phenyl ring and carbonyl group, where as in LUMO+2, electrons are concentrated on phenyl ring and nitrogen atom. These frontier HOMO, LUMO orbital energies are used in the calculation of global reactivity parameters as shown in

Table 7. These parameters tell us about the chemical reactivity and stability of E9 compound [40].

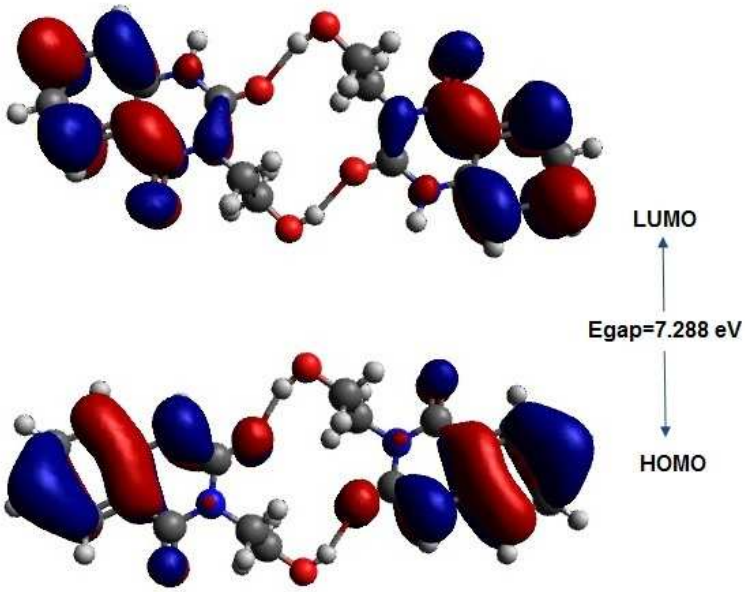

Figure 4. Molecular Orbital Surfaces and Energy Level Gap for the HOMO and LUMO of E9 Dimer

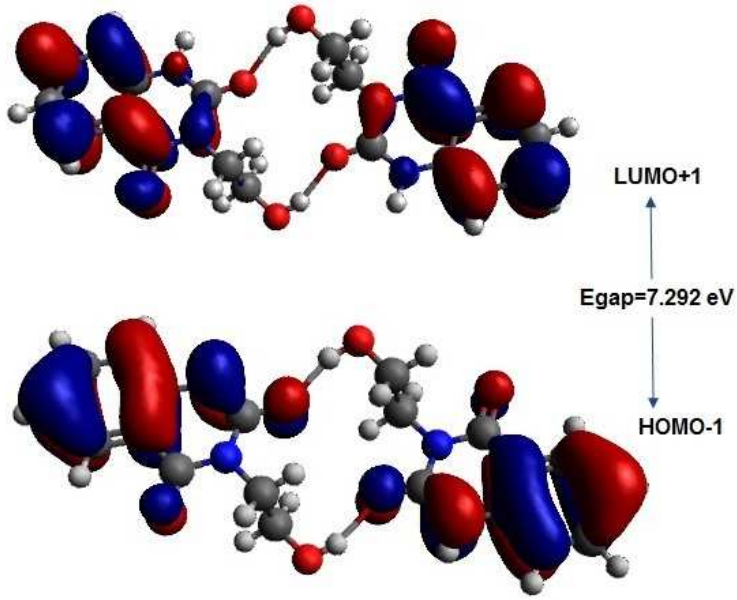

Figure 5. Molecular Orbital Surfaces and Energy Level Gap for the HOMO-1 and LUMO+1 of E9 Dimer

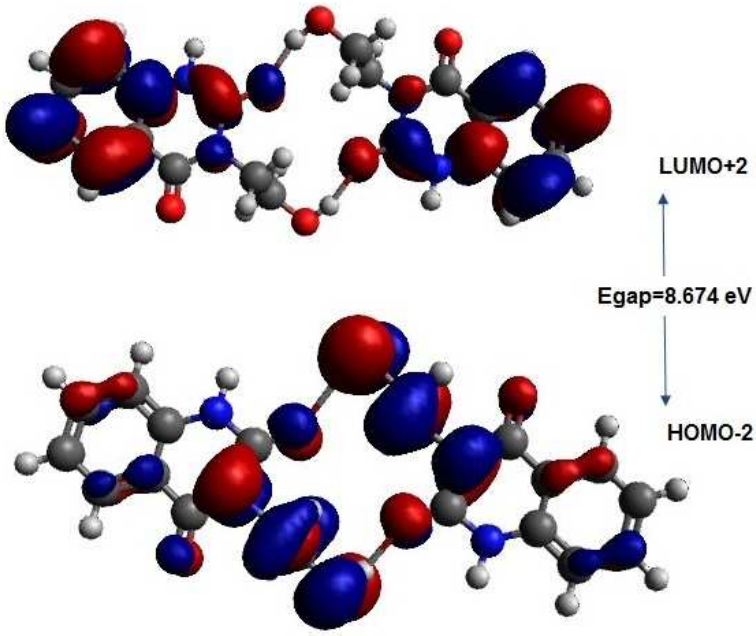

Figure 6. Molecular Orbital Surfaces and Energy Level Gap for the HOMO-2, and LUMO+2 of E9 Dimer

Table 7. Ionization Potential (*I*), Electron Affinity(*A*), Electro negativity (*X*) Chemical Potential (*μ*) Global Hardness (*η*) Global Softness (*s*) and Global Electrophilicity (*ω*) of E9 Dimer

Combinations	A	B
Ionization potential (I)	8.283	8.284
Electron affinity (A)	0.996	0.992
Electro negativity (*X*)	4.639	4.638
Chemical potential (μ)	-4.639	-4.638
Global hardness (η).	3.643	3.646
Global softness (s)	0.1372	0.1371
Global electrophilicity (ω)	2.954	2.950

A= HOMO & LUMO; B= HOMO-1 & LUMO+1

Molecular Electrostatic Potential (MEP)

Molecular electrostatic potential (**Figure 7**) at a point around molecule tell us about the electrostatic effect of electron and proton in molecule which relate with the chemical reactivity and electronegativity of compound. The red color shows that there is negative electrostatic potential and blue color shows that there is positive electrostatic potential. The red color mostly contains electronegative oxygen and nitrogen atoms, whereas blue color contains mostly phenyl ring hydrogen and carbonyl carbon atoms. The potential values show that oxygen act as nucleophilic center and phenyl hydrogen as well as carbonyl carbon act as electrophilic center. These electrostatic potential values tell us about the presence of molecular interactions in a compound [40].

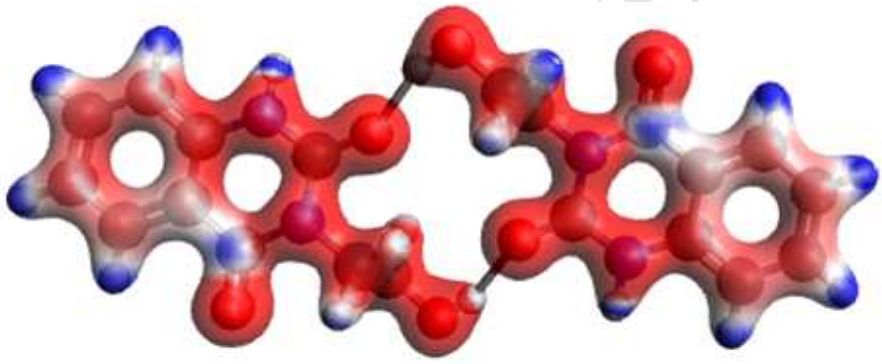

Figure 7. MEP Map of Dimer Calculated at B3LYP/6-31G(d,p) Basis Set

Spectral Characterization of Metal Complexes

FT-IR Characterization of Complexes

The data obtained by FT-IR for characterization of the metal complexes is reported in Table 8. The metal coordination with isatin derived ligand was confirmed by the disappearance of O-H peak at 3430 cm^{-1} and shifting of ν(C-O) peak from 1055 cm^{-1} to lower frequency by 10-19 cm^{-1}, showing the coordination of the oxygen to respective metal [41]. The ν(C=O) peak of isatin moiety was also shifted from 1700 cm^{-1} to 1650-1670 by 30-40 cm^{-1}, indicating the presence of M-O bond [42]. The examination of data showed that ν(C-N) and ν(N-H) peaks are unchanged during complex formation indicating the absence of M-N bond formation. Furthermore the

appearance of new weak peaks of *ν*(M-O) at 473-495 cm^{-1}, showing the formation of metal-ligand bond through oxygen [41]. The origin of a new peak at 3336-3363 cm^{-1} indicated the presence of coordinated water molecule [43]. All these peaks confirmed the formation of metal complexes with isatin derived ligand.

Table 8. FT-IR Data of Metal Complexes

Compounds	**Bond Vibrations (cm^{-1})**						
	***ν*(H_2O)**	***ν*(N-H)**	***ν*(C=O)**	***ν*(C-N)**	***ν*(C-O)**	***ν*(M=O)**	***ν*(M-O)**
E13	3345	3201	1657	1141	1045	-	495
E15	3347	3202	1663	1146	1036	-	478
E18	3336	3189	1670	1139	1044	-	487
E19	-	3180	1661	1140	1043	801	473
E21	3349	3181	1652	1143	1041	-	491
E22	3360	3189	1669	1137	1037	-	475
E23	3358	3202	1658	1143	1040	-	486
E24	3363	3206	1627	1132	1043	-	478

Magnetic Moments of Metal Complexes

The magnetic moment values were recorded using Gouy method for all the metal complexes (**Table 9**). The copper and vanadium complexes (E13, E19) possessed magnetic moments values of 1.95 and 1.78 BM, respectively, showing the presence of one unpaired electron [43]. The magnetic moment of nickel (E15) was 3.19 BM showing the presence of two unpaired electrons. The cobalt metal complex (E18) showed the magnetic moment of 4.38 BM indicating the presence of three unpaired electrons [42]. The chromium complex (E22) showed magnetic moment value of 3.92 BM indicating the presence of three unpaired electrons. The manganese complex (E23) showed magnetic moment value of 5.85 BM indicating the presence of five

unpaired electrons. The iron complex (E24) possessed magnetic moment value of 5.09 BM showing the presence of four unpaired electrons [41]. The zinc complex (E21) was diamagnetic in nature with zero magnetic moment value due to d^{10} system.

Table 9. Magnetic Moments of Metal Complexes

Sr #	Code	Metal	B.M (μ_{eff})
1	E13	Cu(II)	1.95
2	E15	Ni(II)	3.19
3	E18	Co(II)	4.38
4	E19	VO(IV)	1.78
5	E22	Cr(III)	3.92
6	E23	Mn(II)	5.85
7	E24	Fe(II)	5.09
8	E21	Zn(II)	0

Antibacterial Bioassay of Ligand (E9) and Metal Complexes

The antibacterial bioassay was performed on four different bacterial strains as **A** (*Escherichia coli*), **B** (*Staphylococcus aureus*), **C** (*Neisseria gonorrhoeae*) and **D** (*Pseudomonas syringae*) to check the inhibitory activity of ligand and its metal complexes. The agar well diffusion method was used for antibacterial assay in which diameters of inhibition zone were measured in millimeter. The data in **Table 10** and **Figure 8** showed the results of antibacterial activity and these results were compared with standard drug *kanamycin*. DMSO was used as solvent showing no inhibition against any bacterial strain. The bacterial results showed that ligand exhibited remarkable (12 mm) activity against **D**, which was higher than isatin and standard drug *kanamycin*. This showed that ligand was more bactericidal than precursor isatin against **D** bacterial strain. The ligand displayed significant (8-9 mm) activity against **B** and **C,** respectively

while weaker (3 mm) activity was observed against **A** strain. The metal complex (E13) possessed significant (8-10 mm) activity against **B**, **C** and **D** strains and no activity against **A** strain. Also, significant (10 mm) inhibition zone was shown by E15 against **C** and **D** strain and significant (8 mm) against **A** and **B** strain. The complex E17 showed significant (8 mm) activity against **A**, **B** and **D** and showed no activity against **C** strain. Similarly, the E18 complex displayed significant (8-9 mm) activity **C** and **D** and moderate (6 mm) activity was shown by **B** and inactive against **A** bacterial strain. The compound E19 showed significant (8 mm) activity against **D** and **C**, and moderate (6 mm) activity against **B**, respectively. However, E19 complex demonstrated weaker (4 mm) activity against **A** strain. The compound E21 possessed significant (10 mm) activity against **B** and moderate (7 mm) activity against **D**, respectively. The complex E22 was also inactive against **A** and **C,** and showed significant (8 mm) activity against **D** and **B**, respectively. The E23 complex exhibited significant (9 mm) activity against **C,** moderate (7 mm) activity against **B** and **D**, and no activity was observed against **A** strain. Similarly, E24 complex showed significant (8 mm) activity against **B**, moderate (7 mm) activity was shown by **C** and **D** strains and weaker (4 mm) activity against **A** strain. The E25 complex exhibited significant (9-10 mm) activity against **B** and **C**, and no activity against **A** and **D** bacterial strain. The examination of antibacterial data revealed that complexes showed promising activity against **B** and **C** strain as compared to ligand. This increase in activity in complexes was due to metal chelation property [44].

Table 10. Antibacterial Bioassay of Ligand (E9) and Metal Complexes

Sr #	Compounds	Inhibitions Zone (mm)			
		A	B	C	D
1	E9	03	09	08	12
2	E13	Inactive	08	10	08
3	E15	08	08	10	10
4	E17	08	08	Inactive	08
5	E18	Inactive	06	09	08
6	E19	04	06	08	08
7	E21	Inactive	10	Inactive	07
8	E22	Inactive	08	Inactive	08
9	E23	Inactive	07	09	07
10	E24	04	08	07	07
11	E25	Inactive	10	09	Inactive
12	Isatin	12	13	13	08
13	Kanamycin	12	10	12	08
14	DMSO	Inactive	Inactive	Inactive	Inactive

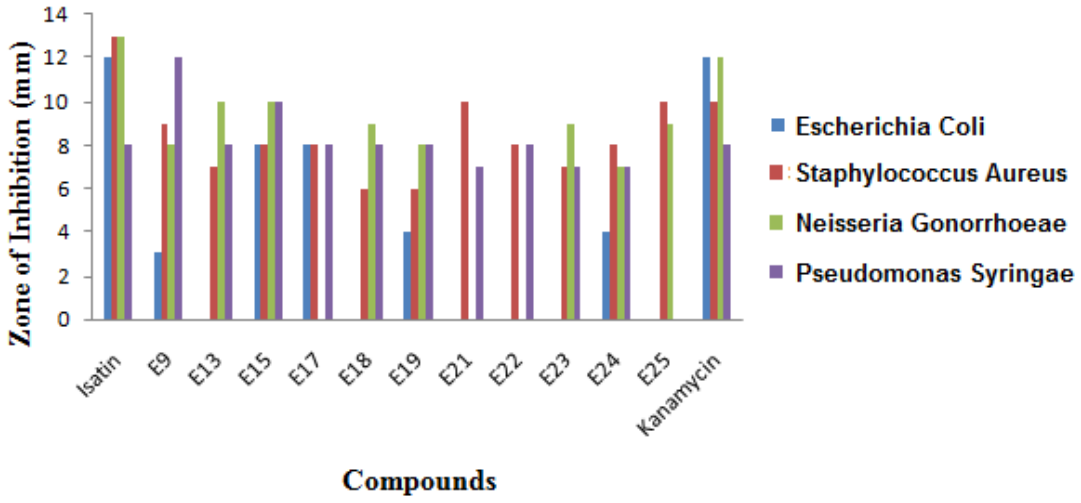

Figure 8. Antibacterial Activity of Ligand (E9) and Metal Complexes Against Four Bacterial Strains

Conclusion

The present research work describes the design and synthesis of isatin based ligand and its metal complexes with first transition series. The ligand was designed by reacting equimolar amount of

isatin and ethanolamine in ethanol at high temperature. The high temperature broke the C-C single bond between two carbonyl carbons of isatin moiety and formation of C-N bond between carbonyl carbons and nitrogen of ethanolamine occurred. The resulting six membered ring formation took place. The structure of ligand was supported by physical (m.p, colour and solubility) and spectral (IR, mass, ^{1}HNMR, ^{1}CNMR and single crystal analysis) data. The DFT calculations were performed for the synthesized crystalline ligand. The computational IR results were compared with experimental IR and hydrogen bonding in ligand was proved with FT-IR findings. The Natural Bond Orbital (NBO) analysis supported the hydrogen bonding results established from IR and explained the inter and intra molecular interactions. The Frontiar Molecular Orbital (FMO) analysis showed the energies of HOMO and LUMO orbitals and these energies were used to find out the global reactivity parameters of ligand. The computed U.V analysis explained the π to π^{*} transition in compound. The bidentate ligand was reacted with transition metal salt of first series to prepare metal complexes. The complexes were characterized by FT-IR and magnetic moment measurements. The octahedral geometry of complexes was observed except vanadium which had square-pyramidal geometry. All the compounds were tested against four bacterial strains and results concluded that most of the metal complexes were more bactericidal than ligand against **B** and **C** bacterial strains due to chelating property of complexes.

Experimental

Materials and Methods

All the required chemicals were of analytical grade and no purification steps were performed except for solvents like ethanol and methanol which were purified. Isatin and ethanolamine were purchased from Sigma Aldrich and Merck, respectively, and used in reaction scheme without further purification. Melting points were taken on Staurt SMP 10, for solvent evaporation purpose rotary evaporator made of Heidolyph was used. For checking the progress of the reaction, TLC was performed using Ultraviolet lamp (UVGL-58, Cambridge, UK). The UV spectra of compounds were recorded on UV-4000, and vibrational characterization was performed on Shimadzu FTIR-8400S Spectrophotometer. Electron impact mass spectrometer instrument made of JEOL MS Route was used to collect fragmentation pattern. ^{1}H and ^{13}C NMR was carried out using Bruker Spectrospin Avance DPX-400MHz using TMS as internal standard and d_6-DMSO as a solvent. The single crystal analysis was performed on Bruker Kappa APEXII CCD diffractometer. ESCO made Laminar Flow Cabinet and Memmert made Incubator was used for antibacterial activity.

Chemistry of Ligand Synthesis

1*H*-Indole-2,3-dione was added in 250 mL two-necked round bottom flask containing 30 mL of ethanol and refluxed for 30 minutes until all the isatin was dissolved until yellowish color solution appeared. Hot ethanolic solution of ethanolamine was added in refluxed isatin solution in an equimolar ratio giving purple color solution which was refluxed for 10 hours and monitored with TLC until brown precipitates produced. The reaction was cooled to room temperature and precipitates collected, washed with ethanol and dried in vacuum to give pure E9. The product was further recrystallized in methanol to give pure brown crystals of E9.

3-(2-hydroxyethyl)quinazoline-2,4(1H,3H)-dione **(E9)**

Yield: (60%); mp 248°C; color (brown); IR (KBr, cm^{-1}): 3430 (O-H), 3200 (NH), 3150 (C-$H_{aromatic}$), 2930 (C-$H_{aliphatic}$), 1700 (C=O), 1550 (C=C), and 1145 (C-N); ^{1}H NMR (ppm d_6-DMSO): δ 3.54 (t, 2H), 3.99 (t, 2H), 4.71 (s, 1H), 7.15-7.92 (m, 4H), 11.31 (s, NH); ^{13}C NMR (DMSO-d_6): δ 42.1, 57.6, 113.8, 114.9, 122.3, 127.3, 134.8, 139.3, 150.2, 162.0; Mass Spectrum (EIMS): $[M]^{+}$ = 206.

Chemistry of Metal Complexes Synthesis

All complexes were prepared using following standard procedure. Ligand (1 mmol) was added in 50 mL two-necked round bottom flask containing 20 mL of methanol. To it added dropwise 10 mL of methanolic solution of respective metal salt (0.5 mmol) and solution was refluxed. Colour changes and precipitate formation occurred during refluxing. The reaction was monitored with TLC. After 7 hours reflux, the mixture was cooled to room temperature, precipitates were collected, washed with fresh methanol, dried in vacuo and recrystallized in mixture of methanol : ethanol (1:1) to give TLC pure respective metal complex.

Computational Procedure

All DFT calculations were carried out with the help of Gaussian 09 program package [45], at the M06-2x/6-31G(d,p) level of theory. The UV–Visible calculations were performed using TD-DFT with B3LYP/6-31G(d,p) method in the gas phase [46, 47]. All the input data files were prepared, using GaussView 5.0 [48, 49]. Finally Chemcraft [50], Avogadro [51] and GaussView 5.0 programs have been used to analyze the output data files.

Biological Studies

In-vitro Antibacterial Bioassay

The antibacterial screening was performed by agar well diffusion method on four different bacterial strains as **A** (*Escherichia coli*), **B** (*Staphylococcus aureus*), **C** (*Neisseria gonorrhoeae*) and **D** (*Pseudomonas syringae*). In these bacteria the **B** was gram-positive and **A**, **C**, **D** were gram-negative. The media (20 g agar, 20 g glucose, 0.2 g $(NH_4)_2SO_4$, 0.2 g KH_2PO_4, 0.05 g $CaCl_2$, 0.05 g $MgSO_4.7H_2O$, 1000 mL dist. H_2O) for bacterial growth was prepared by adding these ingredients in a 2000 mL conical flask and autoclaved at 121 ^oC for one hour. The petri dishes, micropipette tips and filter paper strips were also autoclaved. The recommended samples of concentration 10 mg/250 µL DMSO was prepared. The semi-liquid media was poured in petri dishes, bacterial inoculums were dispersed on the media present in petri dishes with the help of cotton swab. The filter paper strips were placed on each petri dish and samples (10 µL, 400 µg/disc) were injected on these strips with the help of micropipette tips. The control (*Kanamycin*, 10 µL) was also placed on one filter paper strip to see the comparative effect of test sample and control on the inhibition of respective bacteria. The wrapped petri dishes were placed in incubator at 37^oC for 24 hours. After 24 hours, the diameters of inhibition zone were measured in millimeter (mm). The separate DMSO solution was subjected to bacterial activity and results showed that DMSO itself has no activity against any bacteria [52].

Acknowledgments

A.A.C.B (grants #2015/01491-3 and 2014/25770-6) is thankful to Fundação de Amparo à Pesquisa do Estado de São Paulo for financial support. Moreover, Muhammad Khalid (grant # 2017/1314) is thankful to HEC Islamabad Pakistan for financial support.

References

[1] V. P. Modi, D. H. Jani, H. S. Patel, Synthesis and antimicrobial evaluation of spiro compound containing 1,2,4-triazole and isatin, Orbital: Electron. J. Chem. 3 (2011) 68-79.

[2] N. Raman, A. Selvan, S. Sudharsan, Metallation of ethylenediamine based Schiff base with biologically active Cu(II), Ni (II) and Zn(II) ions : synthesis, spectroscopic characterization electrochemical behavior, DNA binding , photonulcease activity and invitro antimicrobial efficacy, Spectrochim. Acta A 79 (2011) 873-883.

[3] J. Devi, S. Kumari, R. Malhotra, Synthesis, spectroscopic studies and biological activity of organosilicon (IV) complexes of ligands derived from 2-aminobenzothiazole derivatives and 2-hydroxy-3-methoxy benzaldehyde, Phosph. Sulf. Sili. Relat. Elem. 187 (2012) 587-597.

[4] J. Devi, N. Batra, R. Malhotra, Ligational behaviour of schiff bases towards transition metal ion and metallation effect on their antibacterial activity, Spectrochim. Acta A 97 (2012) 397-405.

[5] H. L. Singh, J. Singh, Synthesis, spectral, 3D molecular modeling and antibacterial studies of dibutyltin (IV) Schiff base complexes derived from substituted isatin and amino acids, Natur. Sci. 4 (2012) 170.

[6] C.K. Ryu, J. Y. Shim, Y. J. Yi, I. H. Choi, M. J. Chae, J. Y. Han, O. J. Jung, Synthesis and antifungal activity of 5, 8-quinazolinedione derivatives modified at position 6 and 7, Arch. Pharm. Res. 27 (2004) 990–996.

[7] J. A. Sutcliffe, Antibacterial agents: solutions for the evolving problems of resistance, Bioorg. Med. Chem. Lett. 13 (2003) 4159–4161.

[8] M. Verma, S. N. Pandeya, K. N. Singh, J. P. Stables, Anticonvulsant activity of Schiff bases of isatin derivatives, Acta Pharm. 54 (2004) 49-56.

[9] S. N. Pandeya, D. Sriram, G. Nath, E. De Clercq, Synthesis, antibacterial, antifungal and anti-HIV activities of norfloxacin Mannich bases, Eur. J. Med. Chem. 35 (2000) 249-255.

[10] V. Beylin, D. C. Boyles, T. T. Curran, D. Macikenas, R. Parlett, V. Derek, The preparation of two, preclinical amino-quinazolinediones as antibacterial agents, Org. Process. Res. Dev. 11 (2007) 441–449.

[11] J. Feng, Z. Y. Zhang, M. B.Wallace, J. A. Stafford, S. W. Kaldor, D. B. Kassel, M. Navre, L. Shi, R. J. Skene, T. Asakawa, K. Takeuchi, R. Xu, D. R. Webb, S. L. Gwaltney, Discovery of alogliptin: a potant, selective , bioavailable, and efficacious inhibitor of dipeptidyl peptidase (IV), J. Med. Chem. 50 (2007) 2297–2300.

[12] S. K. Sridhar, M. Saravanan, A. Ramesh, Synthesis and antibacterial screening of hydrazones, Schiff and Mannich bases of isatin derivatives, Eur. J. Med. Chem. 36 (2001) 615-625.

[13] S. N. Pandeya, S. Smitha, M. Jyoti, S. K. Sridhar, Biological activities of isatin and its derivatives, Acta Pharmaceutica. 2005, 55 (1), 27–46.

[14] W. Chu, J. Zhang, C. Zeng, et al., N-benzylisatin sulfonamide analogues as potent caspase-3 inhibitors: synthesis, in vitro activity, and molecular modeling studies, J. Med. Chem. 48 (2005) 7637–7647.

[15] W. Chu, J. Rothfuss, Y. Chu, D. Zhou, R. H. Mach, Synthesis and in vitro evaluation of sulfonamide isatin Michael acceptors as small molecule inhibitors of caspase-6, J. Med. Chem. 52 (2009) 2188–2191.

[16] M. C. Pirrung, S. V. Pansare, K. Das Sarma, K. A. Keith, E. R. Kern, Combinatorial optimization of isatin-β-thiosemicarbazones as anti-poxvirus agents, J. Med. Chem. 48 (2005) 3045–3050.

[17] M. J. Konkel, B. Lagu, L. W. Boteju, et al., 3- arylimino-2-indolones are potent and selective galanin GAL3 receptor antagonists, J. Med. Chem. 49 (2006) 3757–3758.

[18] A. Jarrahpour, D. Khalili, E. De Clercq, C. Salmi, J. M. Brunel, Synthesis, antibacterial, antifungal and antiviral activity evaluation of some new bis-Schiff bases of isatin and their derivatives, Molecules. 12 (2007) 1720–1730.

[19] L. Matesic, J. M. Locke, J. B. Bremner, S. G. Pyne, D. Skropeta, M. Ranson, K. L. Vine, N-phenethyl and N-naphthylmethyl isatins and analogues as invitro cytotoxic agents, Bioorg. Med. Chem. 16 (2008) 3118-3124.

20. H. Pervez, M. S. Iqbal, M. Y.Tahir, F.-u.-H. Nasim, M. I. Choudhary, K. M. Khan, In vitro cytotoxic, antibacterial, antifungal and urease inhibitory activities of some N 4-substituted isatin-3-thiosemicarbazones, J. Enz. Inhib. Med. Chem. 23 (2008) 848-854.

[21] K. L. Vine, J. M. Locke, M. Ranson, S. G. Pyne, J. B. Bremner, In vitro cytotoxicity evaluation of some substituted isatin derivatives, Bioorg. Med. Chem. 15 (2007) 931-938.

[22] H. Pervez, M. Ramzan, M. Yaqub, K. Mohammed Khan, Synthesis, cytotoxic and phytotoxic effects of some new N4-aryl substituted isatin-3-thiosemicarbazones, Lett. Drug Des. Discov. 8 (2011) 452-458.

[23] S. N. Pandeya, S. Smitha, M. Jyoti, S. K. Sridhar, Biological activities of isatin and its derivatives, Acta Pharm. 55 (2005) 27-46.

[24] Z. H. Chohan, H. Pervez, A. Rauf, K. M. Khan, C. T. Supuran, Isatin-derived antibacterial and antifungal compounds and their transition metal complexes, J. Enz. Inhib. Med. Chem. 19 (2004) 417-423.

[25] W. Chu, J. Zhang, C. Zeng, J. Rothfuss, Z. Tu, Y. Chu, D. E. Reichert, M. J. Welch, R. H. Mach, N-benzylisatin sulfonamide analogues as potent caspase-3 inhibitors: synthesis, in vitro activity, and molecular modeling studies, J. Med. Chem. 48 (2005) 7637-7647.

[26] W. Chu, J. Rothfuss, Y. Chu, D. Zhou, R. H. Mach, Synthesis and in vitro evaluation of sulfonamide isatin Michael acceptors as small molecule inhibitors of caspase-6, J. Med. Chem. 52 (2009) 2188-2191.

[27] L. Zhou, Y. Liu, W. Zhang, P. Wei, C. Huang, J. Pei, Y. Yuan, L. Lai, Isatin compounds as noncovalent SARS coronavirus 3C-like protease inhibitors, J. Med. Chem. 49 (2006) 3440-3443.

[28] M. C. Pirrung, S. V. Pansare, K. D. Sarma, K. A. Keith, E. R. Kern, Combinatorial optimization of isatin-β-thiosemicarbazones as anti-poxvirus agents, J. Med. Chem. 48 (2005) 3045-3050.

[29] A. Natarajan, Y.-H. Fan, H. Chen, Y. Guo, J. Iyasere, F. Harbinski, W. J. Christ, H. Aktas, J. A. Halperin, 3, 3-Diaryl-1, 3-dihydroindol-2-ones as antiproliferatives mediated by translation initiation inhibition, J. Med. Chem. 47 (2004) 1882-1885.

[30] S.K. Sridhar, S.N. Pandeya, J.P. Stables, A. Ramesh, Anticonvulsant activity of hydrazones, Schiff and Mannich bases of isatin derivatives, Eur. J. Pharm. Sci. 16 (2002) 129.

[31] S. J. Shuttleworth, D. Nasturica, C. Gervais, M. A. Siddiqui, R. F. Rando, N. Lee, Parallel synthesis of isatin-based serine protease inhibitors, Bioorg. Med. Chem. Lett. 10 (2000) 2501-2504.

[32] J. Azizian, M. K. Mohammadi, O. Firuzi, N. Razzaghi-asl, R. Miri, Synthesis, biological activity and docking study of some new isatin Schiff base derivatives, Med. Chem. Res. 21 (2012) 3730-3740.

[33] G. Cerchiaro, A. M. Ferreira, Oxindoles and copper complexes with oxindoles-derivatives as potential pharmacological agents, J. Brazil. Chem. Soc. 17 (2006) 1473.

[34] J. Devi, N. Batra, Synthesis, characterization and antimicrobial activities of mixed ligand transition metal complexes with isatin monohydrazone Schiff base ligands and heterocyclic nitrogen base, Spectrochim. Acta A Mol. Biomol. Spectro. 135 (2015) 710-719.

[35] Q.-G. Ji, D. Yang, Q. Deng, Z.-Q. Ge, L.-J. Yuan, Design, synthesis, and evaluation of novel 1-methyl-3-substituted quinazoline-2, 4-dione derivatives as antimicrobial agents, Med. Chem. Res. 23 (2014) 2169-2177.

[36] A. Casti˜neiras, M. C. F. Vidal, J. Romero, et al., Synthesis, characterization, and magnetic behavior of dinuclear nickel (II) complexes of N,N-substituted dithiooxamides derived from a-amino acids, Zeitschrift fur Anorganische und Allgemeine Chemie. 627 (2001) 1553–1559.

[37] V. Krishnakumar, N. Prabavathi, Analysis of vibrational spectra of 1-chloro-2, 4-dinitrobenzene based on density functional theory calculations, Spectrochim. Acta Mol. Biomol. Spectrosc. 72 (2009) 738-742.

[38] M. Adeel, A.A.C. Braga, M.N. Tahir, F. Haq, M. Khalid, M.A. Halim, Synthesis, X-ray crystallographic, spectroscopic and computational studies of aminothiazole derivatives, J. Mol. Struct. 1131 (2017) 136-148.

[39] C. Ravikumar, I. H. Joe, Electronic absorption and vibrational spectra and nonlinear optical properties of 4-methoxy-2-nitroaniline, Phys. Chem. Chem. Phys. 12 (2010) 9452-9460.

[40] M. N. Arshad, A.M. Al-Dies, A.M. Asiri, M. Khalid, A.S. Birinji, K. A. Al-Amry, A.A. C. Braga, Synthesis, crystal structures, spectroscopic and nonlinear optical properties of chalcone derivative: a combined experimental and theoretical study, J. Mol. Struct. 1141 (2017) 142-156.

[41] M. Xie, L. Gao, L. Li, W. Liu, S. Yan, A new orally active antidiabetic vanadyl complex-bis(alpha-Furancarboxylato)oxovanadium(IV), J. Inorg. Biochem. 99 (2005) 546–551.

[42] M. Shebl, Synthesis, spectral and magnetic studies of mono-and bi-nuclear metal complexes of a new bis (tridentate NO 2) Schiff base ligand derived from 4, 6-diacetylresorcinol and ethanolamine, Spectrochim. Acta A Mol. Biomol. Spectrosc. 73 (2009) 313-323.

[43] M. Shakir, S. Hanif, M. A. Sherwani, O. Mohammad, M. Azam, S. I. Al-Resayes, Pharmacophore hybrid approach of new modulated bis-diimine Cu II/Zn II complexes based on 5-chloro Isatin Schiff base derivatives: Synthesis, spectral studies and comparative biological assessment, J. Photochem. Photobiol. 157 (2016) 39-56.

[44] S. Yasmeen, S. H. Sumrra, M. S. Akram, Z. H. Chohan, Antimicrobial metal-based thiophene derived compounds, J. Enz. Inh. Med. Chem. 32 (2017) 106-112.

[45] M. Frisch,; G. Trucks, H. Schlegel, G. Scuseria, M. Robb, J. Cheeseman, G. Scalmani, V. Barone, B. Mennucci, G. Petersson, Gaussian 09, Revision A. 02; Gaussian, Inc: Wallingford, CT, 2009. 2015.

[46] M. Szafran, A. Komasa, E. Bartoszak-Adamska, Crystal and molecular structure of 4-carboxypiperidinium chloride (4-piperidinecarboxylic acid hydrochloride), J. Mol. Struct. 827 (2007) 101-107.

[47] M.N. Tahir, M. Khalid, A. Islam, S. M. A. Mashhadi, A.A. C. Braga, Facile synthesis, single crystal analysis, and computational studies of sulfanilamide derivatives, J. Mol. Struct. 1127 (2017) 766-776.

[48] M. Frisch, G. Trucks, H. Schlegel, G. Scuseria, M. Robb, J. Cheeseman, G. Scalmani, V. Barone, B. Mennucci, G. Petersson, Gaussian. Inc., Wallingford CT 2009.

[49] E. Frisch, H. Hratchian, R. Dennington, J. TA Keith, B. Millam, Nielsen, J. AJ Holder, Hiscocks, GaussView Version 5.0. 8, Gaussian. Inc: 2009.

[50] C. James, A. A. Raj, R. Reghunathan, V. Jayakumar, I. H. Joe, Structural conformation and vibrational spectroscopic studies of 2, 6-bis (p-N, N-dimethyl benzylidene) cyclohexanone using density functional theory, J. Raman Spectrosc. 37 (2006) 1381-1392.

[51] S. Naseem, M. Khalid, M. N. Tahir, M. A. Halim, A. A. C. Braga, M. M. Naseer, Z. Shafiq, Synthesis, structural, DFT studies, docking and antibacterial activity of a xanthenes based hydrazone ligand, J. Mol. Struct. 1143 (2017) 235-244.

[52] A. U. Rahman, M. I. Choudhary, W. J. Thomsen, Bioassay techniques for drugs development, Harwood Academic Publishers, Amsterdam, The Netherlands, 14 (2001).

Highlights

- Isatin core-based ligand (E9), 3-(2-hydroxyethyl)quinazoline-2,4(1*H*,3*H*)-dione was synthesized by reflux method
- Ligand was characterized by single crystal XRD, IR, NMR and Mass.
- DFT study was performed to explore the electronic property and global reactivity parameters of the ligand
- Transition metal complexes of the ligand were prepared and characterized
- Synthesized compounds were evaluated for bactericidal activity